Simulation study of convective and hydrodynamic turbulent nanofluids by turbulence models

M. Mahdavi, M. Sharifpur[*], JP Meyer

Department of Mechanical and Aeronautical Engineering, University of Pretoria, Private Bag X20, Hatfield, 0028, Pretoria, South Africa.

[*]Corresponding author email: mohsen.sharifpur@up.ac.za

ABSTRACT

The numerical study of nanofluids as a two-phase flow (both as solid nanoparticles and in a liquid phase) has brought about a new approach to simulation in this area. Due to the lack of hybrid models to fully predict the flow characteristics of nanofluids under different conditions, a case can be made for developing homogenous models from numerical simulations. In this study, the convective heat transfer and hydrodynamic characteristics of nanofluids are investigated by simulation with ANSYS-FLUENT. Accordingly, four common types of nanofluids in horizontal turbulent pipe flows have been chosen from experimental data available in literature for modelling purposes. These nanofluids are Al_2O_3, ZrO_2, TiO_2 and SiO_2. The simulations are done using the built-in models of ANSYS-FLUENT, namely the Mixture model and Discrete Phase Modelling (DPM). Comparing various appropriate turbulence models, the Realisable and Standard k-ε models have provided the same results in most of the simulations. The Reynolds stress model (RSM) overestimates pressure drops compared with the other k-ε models, while the re-normalisation group (RNG) model overestimates heat transfer coefficient. The anisotropy of instantaneous velocity in the RSM gives higher turbulent kinetic energy, dissipation rate and slip velocity between the particles and the main flow, which makes it an essential part of simulations. All the DPM results have shown the same trend, but with different percentages from measured data, which means that the number of particles plays a key role in the simulations. Any small weaknesses in DPM have a significant influence on the results due to the higher number of nanoparticles.

Keywords: Nanofluid, numerical simulation, Mixture model, DPM, turbulence

1. Introduction

Boundary conditions, flow field characteristics and changing fluid thermal properties can affect the enhancement of convection heat transfer with nanofluids. The suspension of the nanoparticles in nanofluids creates a larger interaction surface to the volume ratio. Therefore, they can be distributed uniformly to bring about the most effective enhancement of heat transfer without causing a considerable pressure drop. These advantages introduce nanofluids as a desirable heat transfer fluid in the cooling, heating and lubrication industries. The thermal effects of nanofluids in both forced and free convection flows have been studied to a great extent in the last decade. A number of these investigations have been outlined in the review articles [1–3].

Experimental studies show that the variation in the convection heat transfer coefficient for nanofluids is mostly a function of the flow regime, i.e. laminar or turbulent, and the volume fraction of the nanoparticles [4–7]. In the turbulent flow, because of a viscose sublayer close to the heating wall, the impacts of the nanofluids' properties on enhancing the heat transfer rate are extensive under some circumstances [8]. Transporting heat through nanofluids is substantially affected by two principal physical properties: viscosity and conductivity. There is no doubt that an increased nanoparticle concentration results in a rise in both properties, and the change in viscosity is more sensitive than the change in conductivity, as can be expected. Most studies have revealed that an increase in nanoparticle volume fraction has positive effects on the enhancement of heat transfer in forced convection [9–11].

The interaction between dispersed particles and continuous phase is important in turbulent flow because of the instantaneous fluid velocity, which influences the particle trajectory, and affects the flow regime. As a result of a higher order of velocity in turbulence and the nanosized diameter of the particles, gravity might not have a noticeable influence on the fluid flow. Brownian force, which is the major consequence of random motion and collisions with the carrier fluid molecules, also affects particle motion. Brownian motion can be more intense with a decreasing Reynolds number [12]. The effectiveness drops with an increase in bulk viscosity, while it increases with an inflation in temperature [1]. Besides Brownian force, thermophoretic force can be

caused by temperature gradients, which are strongly influenced by the particles' diffusion with different time responses. The drag force over a particle, which is caused by inertia, is also an apparent force in nanofluids. Buongiorno [8] utilises scale analyses to introduce particle time response to each of the forces acting on a particle. Upon comparing the time responses, he concludes that the only major forces would be Brownian and thermophoretic forces. Furthermore, the impact of particle dispersion on turbulent flow and even shear stresses or a fluctuating term of velocity is negligible, and particles always follow the eddies and streamlines. Nevertheless, Xuan and Li [13] have pointed out that the presence of nanoparticles in the flow may expand the turbulence intensity and influence the particle dispersion and turbulence eddy.

Because turbulent flow is more applicable in industry, and turbulence has a larger influence on nanoparticles, many researchers have been interested in experimental studies of nanofluids and heat transfer correlations. Some correlations for Nusselt numbers and friction factors have been investigated for different types of nanoparticles [5, 6, 13–16], but there are many more nanofluids that have not yet been investigated.

Recently, Heyhat, Kowsary, Rashidi, Esfehani, Alem and Amrollahi [17] investigated the thermal and hydrodynamical effects of Al_2O_3 nanoparticles in a fully developed turbulent flow with a constant temperature on the wall in a horizontal tube. Despite the low nanoparticle volume fraction (2%), a 23% increase in heat transfer coefficient was achieved compared with pure water (the base fluid). Changes in the Reynolds number showed no significant effects on heat transfer. The findings of Heyhat et al. [17] illustrated that the pressure drop can be calculated with the traditional correlations that are introduced for pipe flow without nanoparticles. Williams, Buongiorno and Hu [18] also note this about Nusselt number and pressure drop.

There are various models [19, 20] to characterise the improvement of heat transfer in a flow field with nanoparticles injected numerically and theoretically. In a two-phase numerical approach, there are some common methods, including Eulerian-Eulerian and Eulerian-Lagrangian interactions. The Mixture and Eulerian models are two important models of Eulerian-Eulerian interaction. Both the base fluid and particles are considered

to be continuous in the Eulerian model, and governing equations are solved separately for each phase. The Mixture model is like the Eulerian model, which has its own velocity field in each phase and occupies a certain fraction of each specified control volume. This excludes a set of mixture equations that solve iteratively for two phases with a strong coupling. On the other hand, Discrete Phase Modelling (DPM) is the most popular model of Eulerian-Lagrangian interaction for multiphase flows. In this model, the base fluid phase behaves as a continuous phase, and time-averaged Navier-Stokes equations will be solved. The solid phase is estimated by tracking a number of particles into the determined fluid flow by solving the related equation of motion. The exchange of energy, mass and momentum between the continuous and dispersed phases is also predictable. Some researchers explain that it seems unavoidable to neglect the slip velocity between the base fluid and particles due to extra forces, such as Brownian force, in nanofluid flow [13, 21, 22]. Consequently, the two-phase approach may be prescribed for the nanofluid simulations.

A comparison between the single and Mixture models conducted by Bianco, Manc and Nardini [23] and Lotfi, Saboohi and Rashidi [24] in turbulent flow through a circular tube explains that the Mixture model achieves a better agreement with experimental correlation when compared with the single approach. They declared that both the single and Mixture models deliver the same results for a lower volume fraction of nanoparticles, but the difference begins to increase as the particle loading increases. Nonetheless, these studies demonstrated that accurate findings of the model could be reached by improving better correlations for the thermal properties of nanofluids, either experimentally or mathematically. Choosing the right model from literature is another challenge [25].

Huilier [26] compared different auto-correction functions for determining the instantaneous velocity of turbulence and showed that these functions influence the turbulence dispersion of the particles. It is also important to understand which function can properly interpret the real effect of the fluctuating term of the velocity on the particles. Therefore, it is essential to implement a model that captures the effects of

particle dispersion in three directions, although the auto-correlation functions provide the same value for small particles in all directions.

Laín and Sommerfeld [22] employed DPM to calculate the effects of particles with an average diameter of 130 μm for turbulent flow in a pipe. They implemented all the forces that interact between the fluid and the particles. These forces consist of particle inertia, slip-shear lift, slip-rotational lift forces and gravity buoyancy. Laín and Sommerfeld [22] illustrated that reaching a given amount of normalised residuals of velocity or thermal balance is not a proper criterion of convergence solution for Euler-Lagrange calculations. Particle motion equation is solved after a specified number of iterations, and source terms in momentum and energy equations are then updated. Therefore, the residuals iteratively jump to a new amount to again achieve a converged solution for the base fluid flow. Hence, Laín and Sommerfeld [22] compared the changes in velocity and turbulent kinetic energy at a specific place for various steps of given iterations.

Literature shows that most of the numerical studies have focused on a Eulerian-Eulerian approach to nanofluid research and only a few studies have focused on a Lagrangian model of particle flow that considers the interaction between two phases, especially in nanofluids. In this study, two multiphase models, i.e. the Mixture model and DPM, are employed to simulate the thermal enhancement and pressure drop of nanofluid flow in a horizontal tube. To achieve this aim, commercial computational fluid dynamics code FLUENT 15 is operated to solve the governing equations. The geometry and flow conditions of three experimental works (Williams et al. [18], Azmi, Sharma, Sarma, Mamat, Anuar and Rao [27] and Teng, Hung, Jwo, Chen and Jeng [28]) have been considered. The flow in all these works is a turbulent flow in horizontal tubes. The hydrodynamic and heat transfer characteristics of the nanofluids are discussed in the first two studies, as the last study is only concerned with the pressure drop of the nanofluid.

2. Numerical modelling

Four different tube sizes are simulated that are similar to the geometry constructed in Williams et al. [18], Azmi et al. [27] and Teng et al. [28]. Two of these tubes are insulated and only measure the nanofluid pressure drop. The first tube has an inside diameter of 0.01026 m and is 3 m in length [18]. The second tube has an inside diameter of 0.0035 m and is 0.6 m in length [28]. The other two tubes encountered constant heat flux over the outside of the tube. The third tube has an outside diameter of 0.0127 m, an inside diameter of 0.0094 m and is 3 m in length [18]. The fourth tube has an outside diameter of 0.016 m, an inside diameter of 0.019 m and is 1.5 m in length [27]. To produce nanofluids, four different nanoparticles have been suspended in water. These nanoparticles consist of Al_2O_3 [18], ZrO_2 [18], SiO_2 [27] and TiO_2 [28]. The size of the nanoparticles is 46 nm for Al_2O_3, 60 nm for ZrO_2, 20 to 30 nm for TiO_2 (rectangular) and 22 nm for SiO_2. The tests were carried out in turbulent flow up to a Reynolds number of 63 000. In order to ensure the existence of a parabolic axial velocity profile at the entrance of the test section, an extra entrance region similar to the actual physical structure was added to the numerical models as a hydrodynamical section. Mixture models and DPM are employed to solve the effects of nanoparticles in the base fluids.

2.1 Mixture model

The main assumption in the Mixture model is that the robust coupling between particles and fluid, as well as the slip velocity, is not so high. Nevertheless, each phase is assumed to have its own velocity field and to behave as a continuum. Each control volume contains a volume fraction of the primary and secondary phase. The governing equations of this model have been explained in some previous numerical studies [23, 24, 29 and 30].

The mixture continuity, momentum and energy equations are given as follows:

$$\nabla.(\rho_m \vec{u}_m) = 0 , \tag{1}$$

$$\nabla.(\rho_m \vec{u}_m \vec{u}_m) = -\nabla P_m + \nabla.\tau_m + \rho_m g - \nabla.\sum_{k=1}^{2} \varphi_k \rho_k \vec{u}_{km} \vec{u}_{km} , \tag{2}$$

$$\nabla.(\rho_m \vec{u}_m H_m) = -\nabla.(q_m + q_T) - \nabla.\sum_{k=1}^{2} \varphi_k \rho_k \vec{u}_{km} H_k$$
$$+ \nabla.\sum_{k=1}^{2} \varphi_k \tau_k.\nabla \vec{u}_m \qquad (3)$$

$$\tau_m = \nabla.[(\mu_m + \mu_t)(\nabla \vec{u}_m + \nabla \vec{u}_m^T)], \qquad (4)$$

where q_m and q_T are diffusion flux due to conduction and turbulence respectively. It is noted that all the thermophysical properties of the Mixture model are borrowed from experimental work used in this study [18, 27 and 28]. The required constitutive equations are illustrated as follows:

$$\rho_m = \sum_{k=1}^{2} \varphi_k \rho_k, \qquad (5)$$

$$\vec{u}_m = \frac{\sum_{k=1}^{2} \varphi_k \rho_k \vec{u}_{km}}{\rho_m}, \qquad (6)$$

$$\vec{u}_{km} = \vec{u}_k - \vec{u}_m, \qquad (7)$$

$$\vec{u}_{slip} = \frac{\rho_p d_p^2}{18\mu_c f} \frac{(\rho_p - \rho_m)}{\rho_p}\left[\vec{g} - (\vec{u}_m.\nabla)\vec{u}_m - \frac{\partial \vec{u}_m}{\partial t}\right], \qquad (8)$$

$$f = \begin{cases} 1 + 0.15\,\mathrm{Re}_p^{0.687} & \mathrm{Re}_p \leq 1000 \\ 0.0183\,\mathrm{Re}_p^{0.687} & \mathrm{Re}_p > 1000 \end{cases}, \qquad (9)$$

where f is the friction factor (drag function) [31], with the definition of the relative Reynolds number as $\mathrm{Re}_p = \dfrac{d_p \rho_c u_{slip}}{\mu_c}$, where d_p, ρ_c, u_{slip} and μ_m are particle diameter, fluid density, relative velocity between particle and fluid, and fluid viscosity respectively. The drift velocity $\vec{u}_{pm}$ in the binary mixture is given as:

$$\vec{u}_{pm} = \vec{u}_{slip} - \frac{\varphi_p \rho_p}{\rho_m} \vec{u}_{slip} = \frac{\varphi_c \rho_c}{\rho_m} \vec{u}_{slip} \tag{10}$$

The continuity equation of the particle phase provides the distribution of concentration in the fluid as:

$$\nabla.(\varphi_p \vec{u}_m) = -\nabla.(\varphi_p \vec{u}_{pm}) \tag{11}$$

2.2 Discrete phase modelling

In this model, the base fluid is only treated as a continuous phase and the momentum and energy equations are solved, while the secondary phase is tracked by a large number of particles, and the exchange of momentum, energy and mass with the continuous phase can influence the fluid flow. The force balance equation acting on the particle is expressed in a differential form to estimate the trajectory of the particles in the Lagrangian frame:

$$\frac{d\vec{u}_p}{dt} = \frac{3\pi\mu_c d_p f}{m_p}(\vec{u}_c - \vec{u}_p) + \frac{\vec{g}(\rho_p - \rho_c)}{\rho_p} + \vec{F}_{other} \tag{12}$$

A simple scale analysis can easily present the order of slip velocity $\vec{u}_{slip} = \vec{u}_p - \vec{u}_c$. By comparing only the drag force and inertia of the particle, as well as assuming the order of $\frac{du}{dt} \sim \frac{U}{t}$, one finds:

$$u_{slip} \sim \frac{\tau}{ft}U, \tag{13}$$

$$\tau = \frac{\rho_p d_p^2}{18\mu_c}, \tag{14}$$

$$t = \frac{L}{U}, \tag{15}$$

where L and U are the characteristic length and velocity of the fluid [32]. In this study, inlet velocity and tube diameter were chosen as U and L respectively. By defining the Stokes number as the ratio of particle relaxation time τ to fluid response time and the fact that friction factor is at the order of unity $f \sim O(1)$ from previous sections, or even for the case of the Stokes regime $f=1$, it can find:

$$u_{slip} \sim O(StU) \tag{16}$$

Since all the parameters were available from experimentation in literature [18, 27 and 28], it was revealed that the order of slip velocity is 10^{-5} as $u_{slip} \sim O(10^{-5})$.

In this approach, the friction factor is redefined as:

$$f = \frac{C_D \, \text{Re}_p}{24} \tag{17}$$

Drag coefficient C_D is presented for smooth spherical particles [33]:

$$C_D = a_1 + \frac{a_2}{\text{Re}_p} + \frac{a_3}{\text{Re}_p^2}, \tag{18}$$

where constant values a_1, a_2 and a_3 are used for a wide range of Reynolds numbers. For rectangular particles, d_p and shape factor are defined. Therefore, the drag coefficient is as follows [34]:

$$C_D = \frac{24}{\text{Re}_p}(1 + b_1 \, \text{Re}_p^{b_2}) + \frac{b_3 \, \text{Re}_p}{b_4 + \text{Re}_p}, \tag{19}$$

where b_i ($i=1, 2, 3$ and 4) constants are a function of shape factor θ as:

$$\theta = \frac{a}{A}, \tag{20}$$

$$b_1 = \exp(2.3288 - 6.4581\theta + 2.4486\theta^2), \tag{21}$$

$$b_2 = 0.0964 + 0.5565\theta, \tag{22}$$

$$b_3 = \exp(4.905 - 13.8944\theta + 18.4222\theta^2 - 10.2599\theta^3), \tag{23}$$

$$b_4 = \exp(1.4681 + 12.258\theta - 20.7322\theta^2 + 15.8855\theta^3), \tag{24}$$

where a and A are the surface of a spherical particle with the same volume as the actual particle and surface area of the particle respectively.

Other forces that affect the particle include the following:

- Gravity force
- Virtual mass caused by the acceleration of the fluid around the particle
- Force due to pressure gradient
- Brownian force caused by the random motion of particles through the base fluid (this usually has a weak effect on flows with higher velocity)
- Lift force due to shear stress and thermophoretic force due to a temperature gradient [32]

Virtual mass force:

$$\vec{F}_{vm} = 0.5 m_p \frac{\rho_c}{\rho_p}\left(\vec{u}_p \nabla \vec{u}_c - \frac{d\vec{u}_p}{dt}\right), \tag{25}$$

Pressure gradient force:

$$\vec{F}_p = m_p \frac{\rho_c}{\rho_p} \vec{u}_p \nabla \vec{u}_c, \tag{26}$$

Brownian force:

$$\vec{F}_B = \vec{\varsigma}\sqrt{\frac{6\pi\mu_c d_p K_B T}{\Delta t}} \; ,$$ (27)

where $\vec{\varsigma}$ is the Gaussian random vector function with zero mean value and Δt Lagrangian time step. The key factor to use this correlation is the assumption of continuum in the fluid medium. Considering that the mean free path of water is about $\lambda=0.3$ nm and the particle diameter is 22 to 60 nm in this study, the Knudsen number $Kn= \lambda/d_p$ results to $Kn<0.1$, which is valid for the continuum medium.

Lift force with d_{ij} as deformation tensor:

$$\vec{F}_L = \frac{5.188 m_p \mu_c^{0.5} \rho_c^{0.5} d_{ij}}{\rho_p d_p (d_{lk} d_{kl})^{0.25}} (\vec{u}_c - \vec{u}_p)$$ (28)

A correlation for thermophoretic velocity is available from the experimental work of McNab and Meisen [35]. The use of this correlation in this study raises some doubt, as it has been presented for particles with the order of μm diameters. However, this is the only available correlation for the binary of liquid and solid particles. With the definition of thermophoretic velocity, the thermophoretic force can be derived by Stokes's drag force as follows:

$$u_T = -0.26 \frac{\mu_c}{\rho_c} \frac{\kappa_c}{2\kappa_c + \kappa_p} \frac{\nabla T}{T} \; ,$$ (29)

$$F_T = -3\pi d_p \mu_c V_T = -D_T \frac{\nabla T}{T} \; ,$$ (30)

$$D_T = 0.78 \frac{\pi\mu_c^2 d_p}{\rho_c} \frac{\kappa_c}{2\kappa_c + \kappa_p} \; ,$$ (31)

where u_T, F_T and D_T are thermophoretic velocity, force and coefficient respectively; κ_p is particle thermal conductivity, and μ_c, ρ_c and κ_c are fluid viscosity, density and thermal conductivity respectively. The balance of heat transfer for each particle is:

$$m_p c_p \frac{dT_p}{dt} = hA \ (T_c - T_p) \tag{32}$$

The heat transfer coefficient of flow over a particle is available by the following correlation [36]:

$$\frac{hd_p}{\kappa_c} = 2 + 0.6 \operatorname{Re}_p^{0.5} \operatorname{Pr}^{1/3} , \tag{33}$$

where Pr is the Prandtl number of the base fluid.

The influence of particle motion on the base fluid can be seen in the momentum and energy equations of two source terms. The momentum source term consists of the drag and other exchange forces, and the energy source term is computed from the energy balance for a particle in each computational cell.

Momentum source term as a force:

$$F_s = \sum (\frac{18\mu_c}{\rho_p d_p^2} \frac{C_D \operatorname{Re}_p}{24} (\vec{u}_p - \vec{u}_c) + \vec{F}_{other}) \dot{m}_p \Delta t \tag{34}$$

It is noted that the amount of particle mass flow rate $\dot{m}_p$ is preserved in each Lagrangian iteration. The energy source term is computed as:

$$Q_s = \dot{m}_p c_p (T_{p_{in-cell}} - T_{p_{out-cell}}) , \tag{35}$$

where $T_{p_{in-cell}}$ and $T_{p_{out-cell}}$ are the particle temperature at the inlet and outlet of each computational cell.

2.3 Turbulence modelling

Due to the ultrafine size of the nanoparticles, it could be claimed that the instantaneous fluctuation of the velocity field affects particle trajectories, which eventually changes the pressure and velocity field in turbulent flow. Therefore, the Discrete Random Walk (DRW) model [37] is employed as a stochastic method to simulate the impacts of a fluctuating term of velocity. Some researchers have successfully employed this model [38, 39]. However, in this study, the turbulence dispersion of the particles and the effects of this dispersion on flow field are taken into account simultaneously as the two-coupling. Gaussian probability density function (pdf) is used to introduce the random fluctuating value of velocity V_i' during eddy lifetime as:

$$u_i' = \zeta \sqrt{\overline{u_i'^2}} \,, \tag{36}$$

where ζ is the randomly distributed number from the Gaussian pdf and $\sqrt{\overline{u_i'^2}}$ is the root mean square of fluctuating velocity in each direction. The amount of fluctuating velocity can be defined [40] as $\sqrt{\overline{u_i'^2}} = \sqrt{\dfrac{2}{3}k}$, where k is the kinetic energy of turbulence. The assumption of isotropy is only applicable in the $k-\varepsilon$ turbulence model, while the Reynolds stress model (RSM) presents different fluctuating velocities in each direction. There are two characteristic times that the fluctuating velocity value is constant, with the minimum difference being during the lifetime of the eddy and during the particle eddy crossing time. The interaction between the eddy and the particle occurs during this period. At the end of the period, a new location for the particle and a new amount of ζ are set to obtain the new particle velocity by using the new local fluctuating fluid velocity.

Three different $k-\varepsilon$ turbulence models have been employed to simulate the fluid flows that are appropriate for the smooth tubes of the chosen experimental works [27 and 41]. They consist of Standard [42], re-normalisation group (RNG) [43] and Realisable [44] $k-\varepsilon$ models. On the other hand, the roughness value of the tube used in the experimental work of Teng et al. [28] is 4.6×10^{-5} m, which affects the flow and pressure drop. The $k-\omega$ turbulence model involves the effect of roughness in the boundary layer. Therefore, the $k-\omega$ Shear Stress Transport (SST) [45] turbulence model is employed in this case. Assuming the same fluctuating velocity value in all directions (or isotropy assumption) in the DRW model by $k-\varepsilon$ models may produce some errors in the calculation of instantaneous velocity, especially in the boundary layer. Consequently, the RSM or Large Eddy Simulation (LES) can be more accurate [46 and 47]. Thus, the RSM has been employed to simulate turbulence in this study as well.

2.4 Model geometry, boundary conditions and numerical method

All the geometries have extra entrance (>30D) to ensure the existence of fully developed flow at the test section. The study of both two-dimensional (2D) axisymmetric and three-dimensional (3D) models seems essential to understand the abilities of the turbulence models, especially in the Lagrangian approach. Therefore, the results of both simulations are briefly discussed to present an appropriate geometry model. Due to a clear discrepancy between fine and coarse mesh results in the vicinity of the wall, a standard wall function model cannot properly capture the influences of the viscous sublayer in the velocity field.

On the other hand, the influence of the intense gradient on mean velocity and fluctuating velocity in each direction in the boundary layer on particles is inevitable.

As a result, an enhanced wall treatment model has been chosen for all models, with fine mesh at the entrance and six to ten nodes in the viscous boundary layer [48]. FLUENT 15 [49] was employed to solve the governing equations with the control volume approach. The SIMPLE method was used to couple pressure and velocity in equations. The QUICK scheme was employed for volume fraction and Second Order Upwind for other parameters to discretise the governing partial differential equations. Several kinds

of structured non-uniform grids were generated to ensure the accuracy of grid independency. For all of them, the amount of y^+ in the first node (adjacent to the wall) was between 0.7 and 1.2, which is the appropriate y^+ for the enhanced wall treatment model. The source terms of momentum and energy are renewed in DPM after a specified number of iterations. Therefore, the residuals jump to reach a converged solution again. The evolution of velocity profile and pressure drop at a reference location in each case was considered as a convergence criterion. Because of the length of the tube (which is relatively long), it is important to ensure that all the particles have escaped from the outlet by setting a proper maximum number of time steps, which is more than 10^4 in this study.

In order to include the impact of instantaneous velocity on particles, a statistical distribution of particle trajectories is computed in each computational cell or parcel, especially in the case of a higher volume fraction. This distribution is presented as the number of tries in which no change in the results is observed when it is set to more than 15 for the highest particle loading in this study.

Due to a high number of nanoparticles in each parcel (in the order of 10^{10}), there is a major difference between the injection of nanoparticles and the injection of other kinds of particles. Because of boundary layer formation, there is considerable slip velocity between the base fluid and particles at the beginning of the calculations in the entrance region, which produces noticeable force in the momentum source term. The forces are calculated for a single particle and then multiplied by the number of particles in each parcel. Thus, it is crucial to reduce the source term relaxation factor and update it many times.

3. Results and discussion

A comparison between 2D and 3D results reveals that, with the exception of the RSM, two-equation turbulence models exhibit almost similar trends and values of findings in both 2D and 3D results, with the difference being less than 6%. On the other hand, a gap between RSM results in 2D and 3D with DPM was observed. It showed that the assumption of anisotropy in 3D has non-negligible effects on particle dispersion and flow field. Thus, the 3D model is employed as a general geometry for all the

simulations. The Standard and Realisable models have shown the same behaviour in calculations, while the RNG model shows similar results in the calculation of pressure drop and overestimates heat transfer coefficient.

At the beginning of this section, the amount of uncertainty from the experimental works is presented for further discussion in Table 1. There are only some doubts about the uncertainty of heat transfer coefficient calculated by Azmi et al. [27]. They stated the precision of the thermocouples as ± 0.1 ℃. Regarding the temperature difference between wall and fluid bulk from 1.5 ℃ to 2.5 ℃ in their tests, the uncertainty may go beyond 9%.

Table 1: Uncertainty analysis of measured pressure drop and heat transfer

	Williams et al. [18]	Azmi et al. [27]	Teng et al. [28]
Pressure drop	0.5%	1%	
Heat transfer coefficient	<10%	0.8%	<6%
Reynolds number	<1%	<1%	

The comparison of the pressure losses and heat transfer coefficient of the turbulence models with experimental measurement is shown in Figure 1. On the other hand, the abilities of two multiphase models, i.e. the Mixture model and DPM, have to be studied. As a result, the application of both the turbulence and multiphase models are discussed at the same time. Also, 10% error bars were added to the experimental results to provide a better understanding of the difference with numerical simulations.

The pressure drop and heat transfer coefficient for heated tubes without nanoparticles are illustrated in Figure 1. All the k-ε models are in good agreement with experimental results for predicting pressure drop. However, the RSM prediction for pressure loss indicates a 14 to 16% difference from experimental results (lower to higher Reynolds numbers). The RSM estimates the heat transfer coefficient with high precision. Despite good prediction of pressure loss by the RNG model, this model overestimated heat transfer coefficient by 12%.
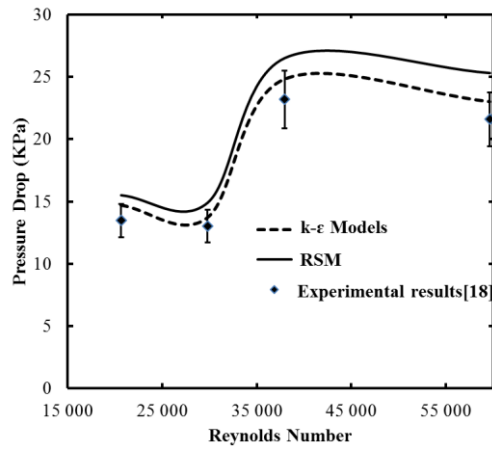
a)
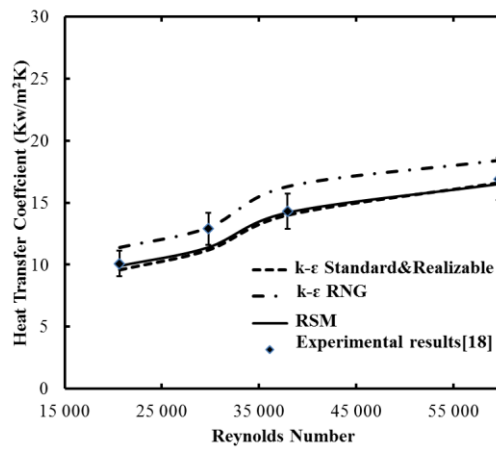
b)

Figure 1: a) Pressure loss and b) heat transfer coefficient in the heated tube without nanoparticles.
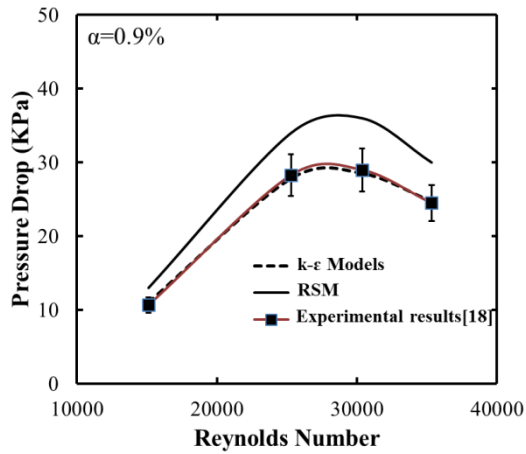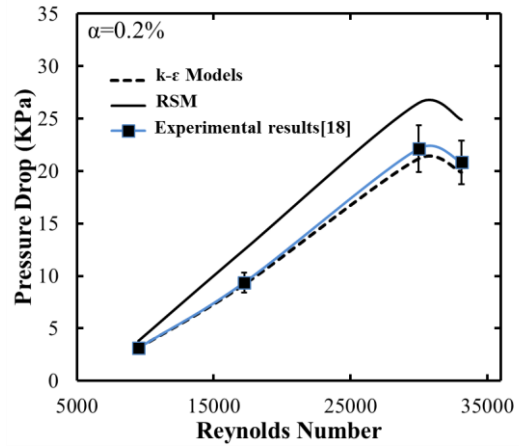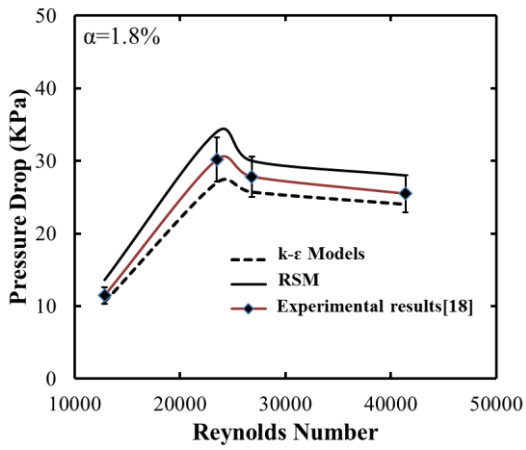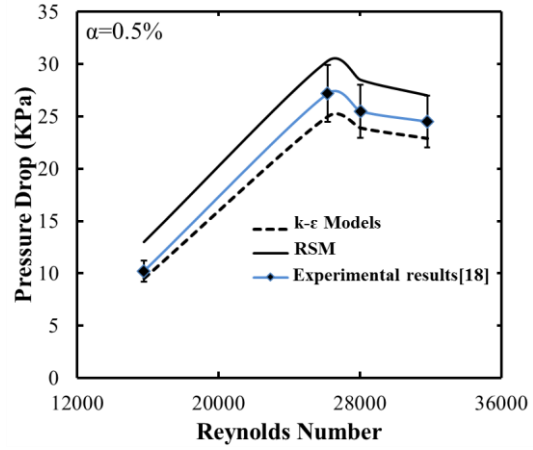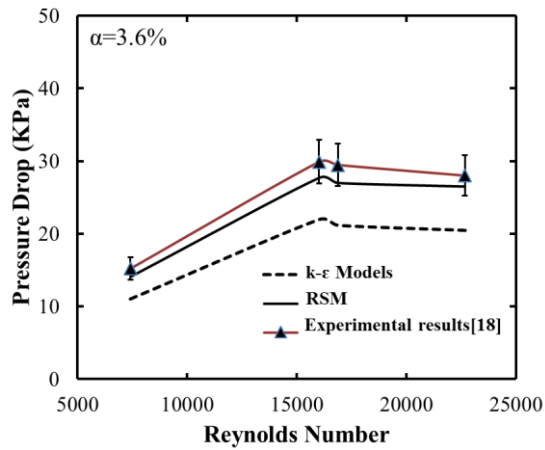
Figure 2: A DPM prediction of pressure drop in an insulated tube with a), b) and c) Al_2O_3 and d), e) and f) ZrO_2 nanofluid flow with a different particle loading.
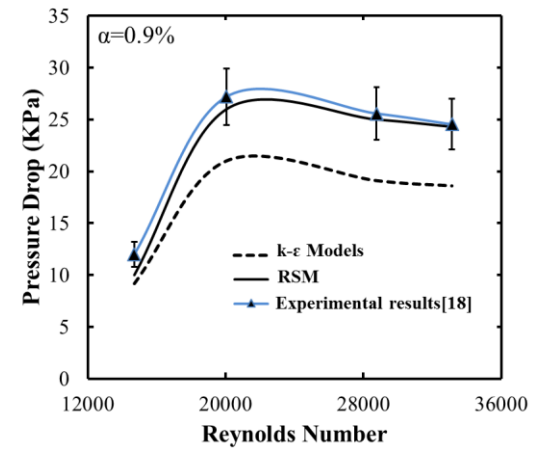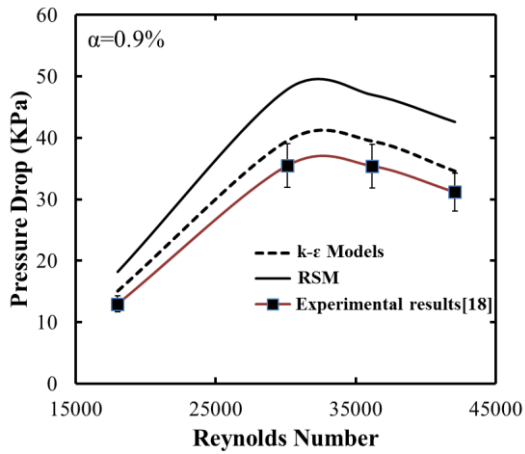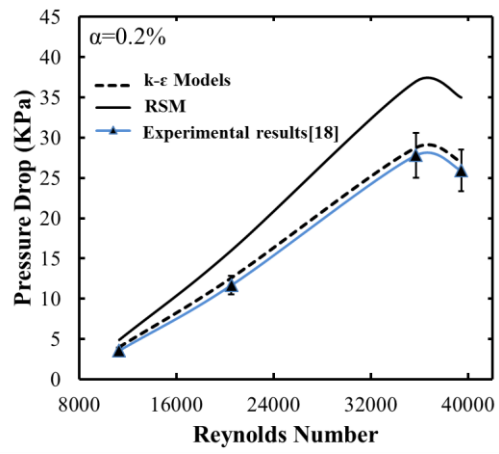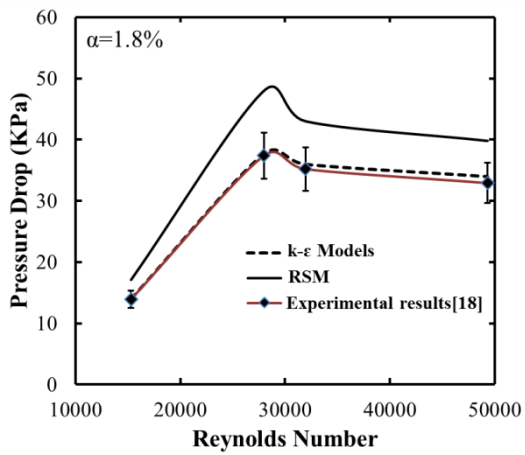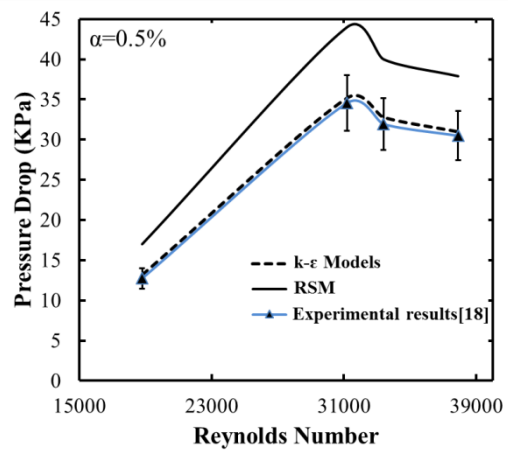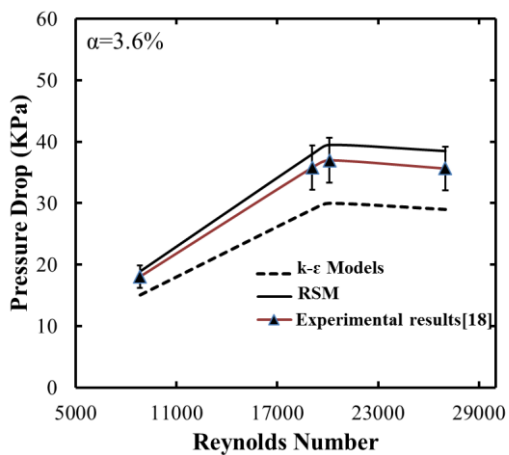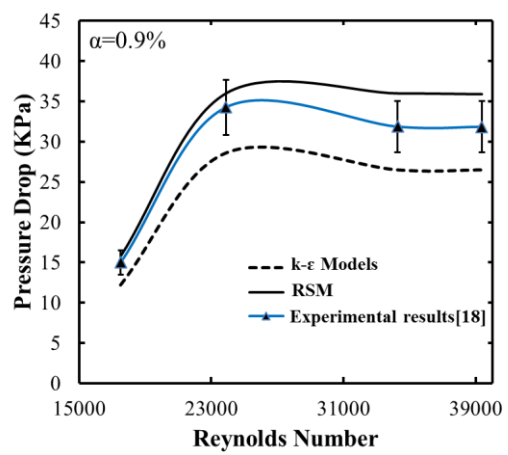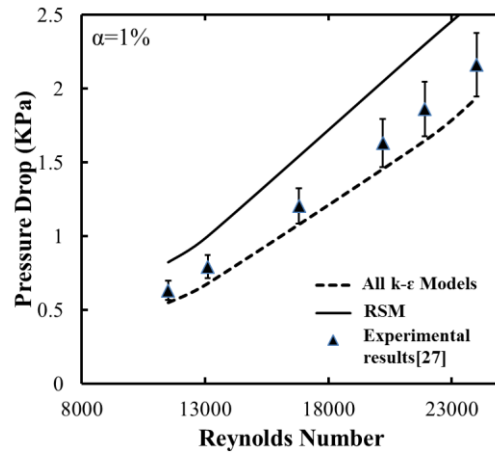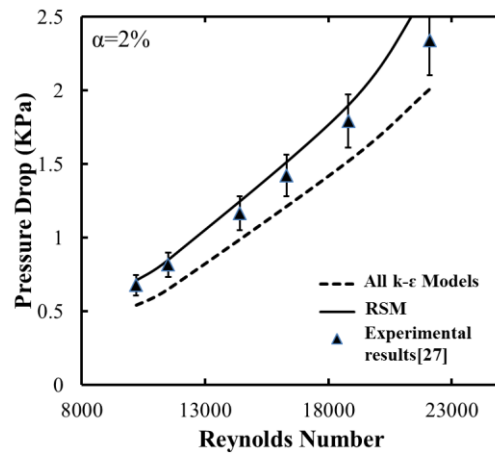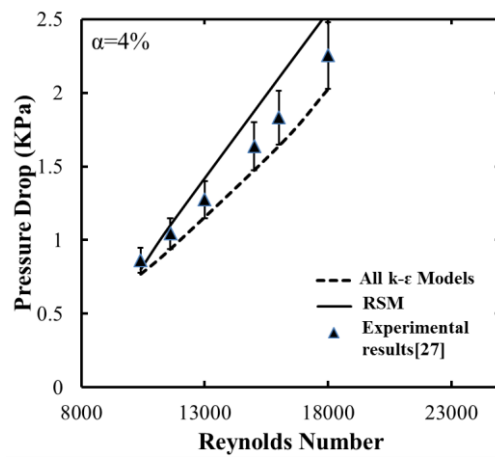
a)

b)

c)

d)

e)

f)

Figure 3: A DPM prediction of pressure drop in a heated tube with a), b) and c) Al_2O_3 and d), e) and f) ZrO_2 nanofluid flow with a different particle loading.
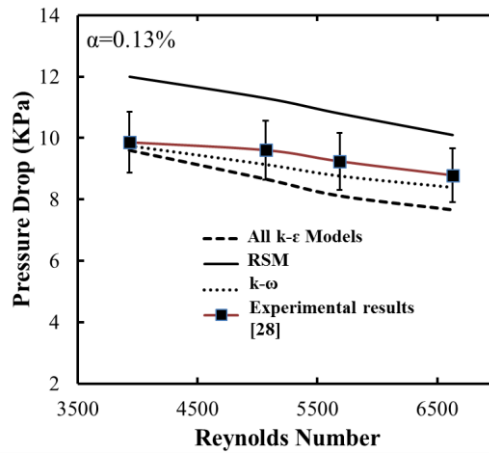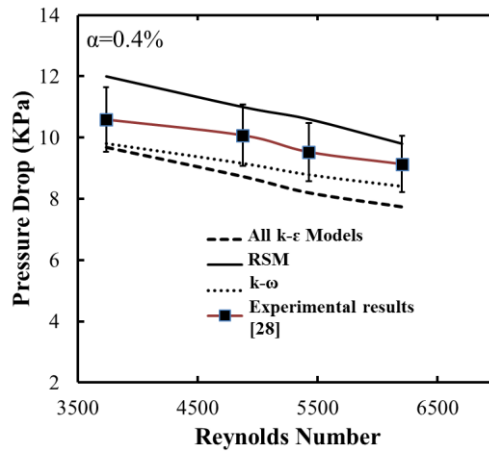
a)

b)

c)

Figure 4: A DPM prediction of pressure drop through a heated tube flow with SiO_2 nanoparticles with a different particle loading.

The DPM estimation of pressure drop in both adiabatic and diabatic tubes is presented in figures 2 to 5. In order to provide a comparison between the graphs, three orders of magnitude for the Reynolds number can be recognised as a higher Reynolds number above 18 000 [18], an intermediate Reynolds number between 12 000 and 18 000 [27] and a lower Reynolds number less than 12 000 [28].

a)

b)

Figure 5: A DPM prediction of pressure drop through an isolated tube flow with TiO_2 nanoparticles with a different particle loading.

A pressure drop trend in both heated and adiabatic tubes with Al_2O_3 and ZrO_2 nanofluids is evident in figures 2 and 3. The discrepancy will be particularly noticeable with the expanding Reynolds number. With a lower particle volume fraction in the adiabatic tube in Figure 2, RSM overestimates pressure loss with a difference of almost 17% in both Al_2O_3 and ZrO_2 nanofluids. By increasing the particle loading, k-ε models start

underpredicting pressure drops, especially at a volume fraction of 3.6% in Al_2O_3 and 0.9% in ZrO_2 nanofluids. At this volume fraction, the experimental pressure drops are at the maximum difference with simulation results by k-ε models and closer to RSM (22% by k-ε models and 4% by RSM in average). The trend is almost the same in the heated tube, which is shown in Figure 3. This means that, at a lower volume fraction, the k-ε models are capable of more accurately predicting pressure drops. This might come from the fact that k-ε models and RSM have different points of view of turbulence. The former assumes the same amount of Reynolds stresses in all directions, while the latter applies different values in each direction. In other words, the effects of the anisotropy of fluctuating velocity on particles needs to be properly captured by RSM. This anisotropy may present some poor prediction in lower particle volume fractions and higher Reynolds numbers.

Pressure drops in the range of intermediate Reynolds numbers (12 000 to 18 000) are presented in Figure 4 under constant heat flux. The changes of RSM results in respect of the increase in particle volume fraction are more sensible than k-ε model predictions. This proves that RSM can capture the influences of an increase in particle volume fraction better than k-ε models. A similar explanation can be stated for the experimental study of Teng et al. [28] in the low range of particle loading and lower Reynolds numbers (3 000 to 6 500), as shown in Figure 5. The impact of roughness used in the k-ω model is also important and, at a lower particle loading, the k-ω model predictions are in better agreement with experimental data.

Pressure drop predicted by the Mixture model in adiabatic and diabatic tubes for different nanoparticles is presented in figures 6 to 9. Since the thermophysical properties implemented in the Mixture model come from the experimental measurements, a good agreement between simulation results and data from the tests is anticipated in most of the cases, especially for the Reynolds numbers less than 18 000 in figures 6 and 7. Pressure losses estimated by k-ε models and RSM have shown a good match with experimental data for Reynolds numbers less than 18 000 in figures 6 and 7, whereas for higher Reynolds numbers, RSM overestimates the results. This can also be observed in the range of intermediate Reynolds numbers for heated tubes with SiO_2 nanoparticles in Figure 8. In this range of Reynolds numbers, the entire simulation

results and measured data have provided almost the same value for various amounts of particle loading.
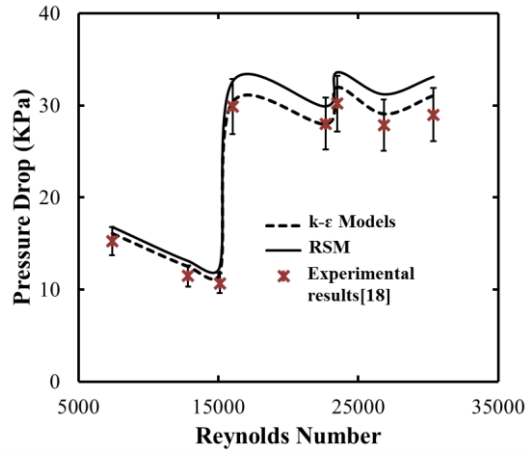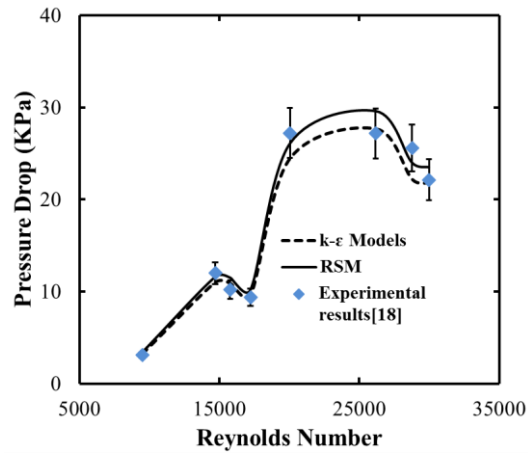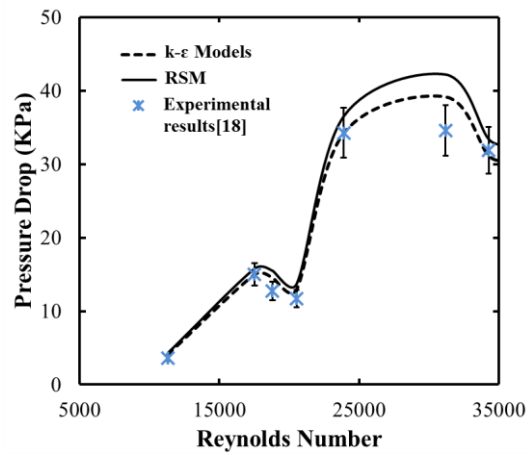

a)
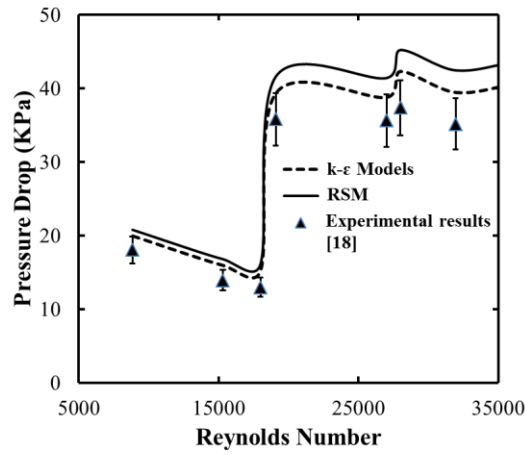
b)

Figure 6: A Mixture model prediction of pressure drop through a) an isolated and b) a heated tube with Al_2O_3 nanofluid flow.

It seems that the effect of roughness in experimental work by Teng et al. [28] is appreciable, as predicted by the k-ω model in Figure 9. The physical properties of the TiO_2 nanofluid are employed from the measured data [28]. The difference between the simulation and the experimental results is 7% for k-ε models and 4% for k-ω models and RSM.

a)

b)

Figure 7: A Mixture model prediction of pressure drop through a) an isolated and b) a heated tube with ZrO_2 nanofluid flow.
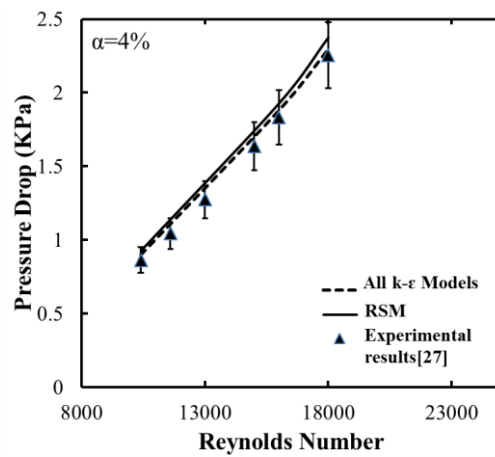
The results of the simulation for heat transfer coefficients are described in figures 10 to 13. The figures show a similar pattern in DPM estimations for Al_2O_3, ZrO_2 and SiO_2 nanofluids. In all the simulations, the RNG model overestimated the heat transfer coefficient. Therefore, it is not appropriate for characterising heat transfer parameters.
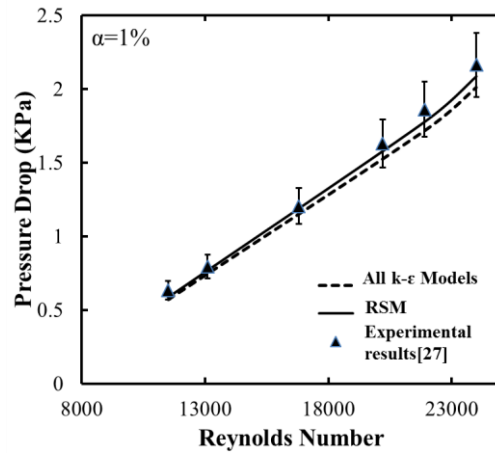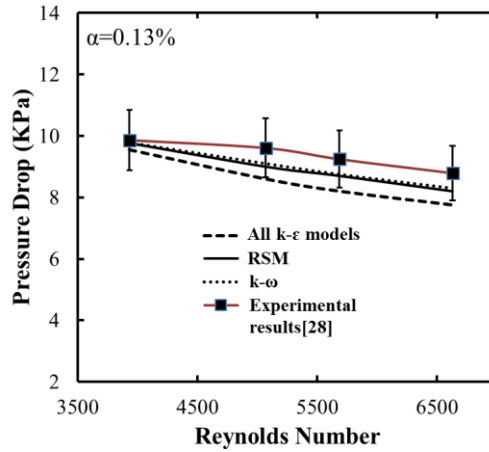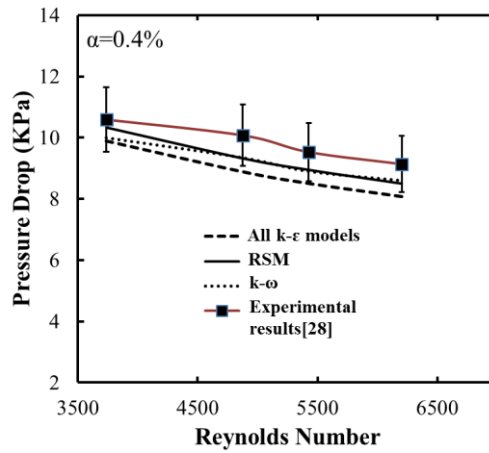
a)
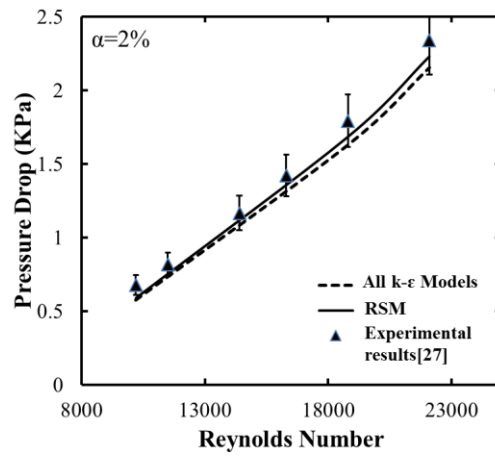
b)

c)

Figure 8: A Mixture model prediction of pressure drop through a heated tube flow with SiO$_2$ nanoparticles.

a)

b)

Figure 9: A Mixture model prediction of pressure drop through a heated tube flow with TiO$_2$ nanoparticles.

The *k-ε* Standard and Realisable models, as well as RSM, have shown good agreement with measured data in the low volume fraction of Al$_2$O$_3$ and ZrO$_2$ nanoparticles in Figure 10. With regard to experimental results, the difference between those models rises with an increase in nanoparticle loading and reaches 35% for Al$_2$O$_3$ and 30% for ZrO$_2$ for 3.6% and 0.9% volume fraction respectively. The SiO$_2$ nanofluid in Figure 11 exhibits a similar trend, and the difference is 20% for 4% volume fraction, which indicates that the error will be less for lower Reynolds numbers. Nonetheless, the numerical results are in the range of 10% uncertainty, except for $\varphi_p > 2\%$ in Al$_2$O$_3$, $\varphi_p > 0.5\%$ in ZrO$_2$ and $\varphi_p > 2\%$ in SiO$_2$ nanofluids.
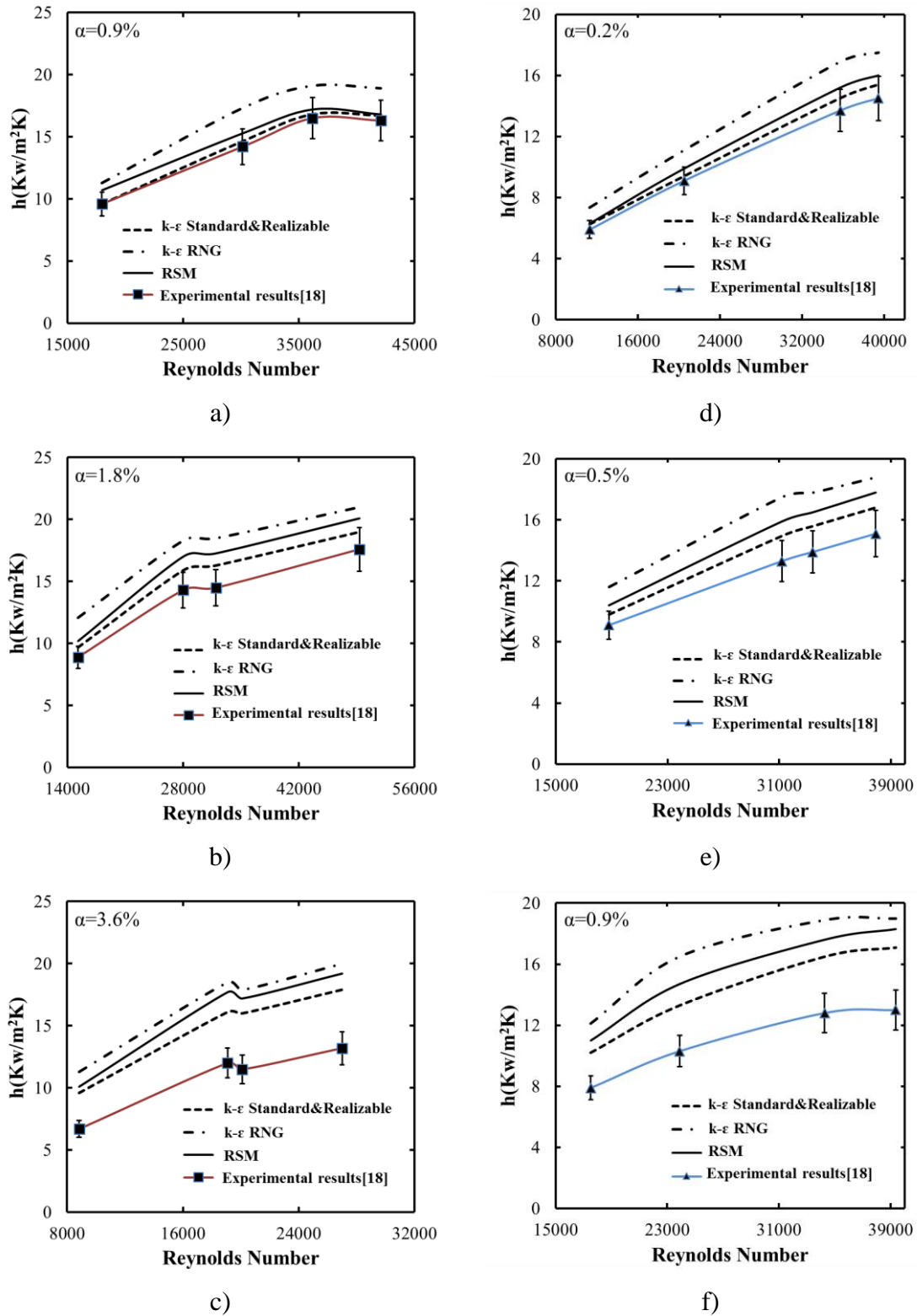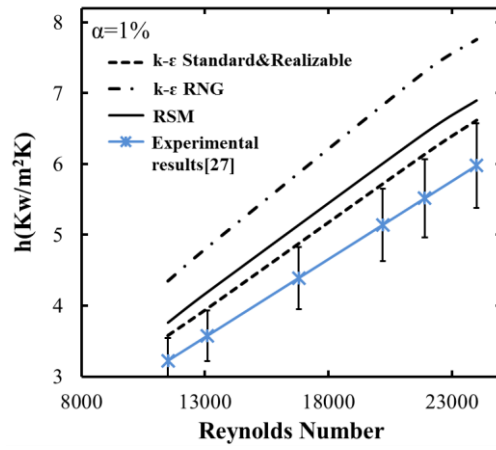
Figure 10: A DPM prediction of heat transfer coefficient through a heated tube with a), b) and c) Al_2O_3 and d), e) and f) ZrO_2 nanofluids with a different particle loading.

a)
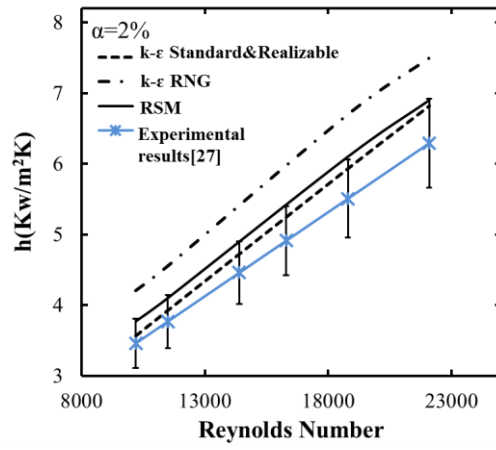
b)
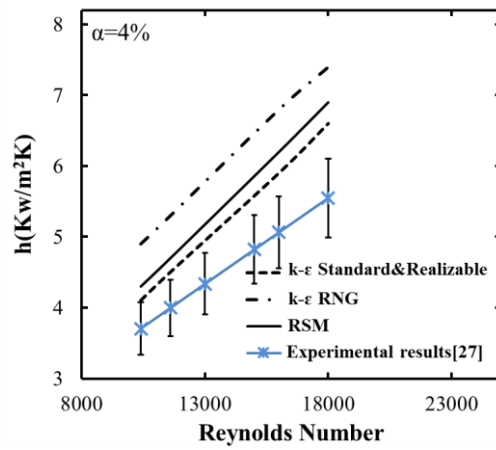
c)

Figure 11: A DPM prediction of heat transfer coefficient of SiO_2 nanofluid through a heated tube with a different particle loading.

Simulation results of heat transfer coefficient by the Mixture model are illustrated in figures 12 and 13. The Mixture model is more accurate in predicting heat transfer characteristics. It seems that the thermophysical properties introduced for mixture fluid are appropriate for nanofluid as well. Again, the RNG model cannot be recommended for estimating heat transfer coefficient.

a)

b)

Figure 12: A Mixture model prediction of heat transfer coefficient through a heated tube with a) Al_2O_3 and b) ZrO_2 nanofluids.
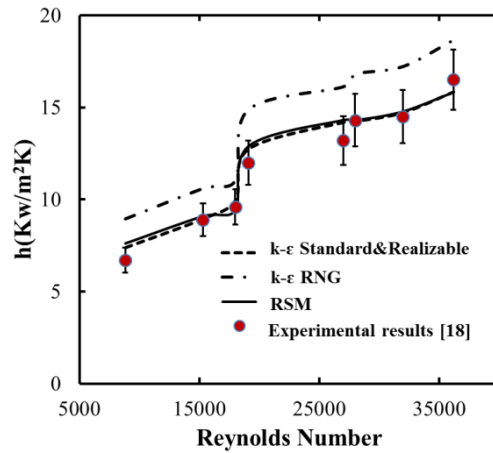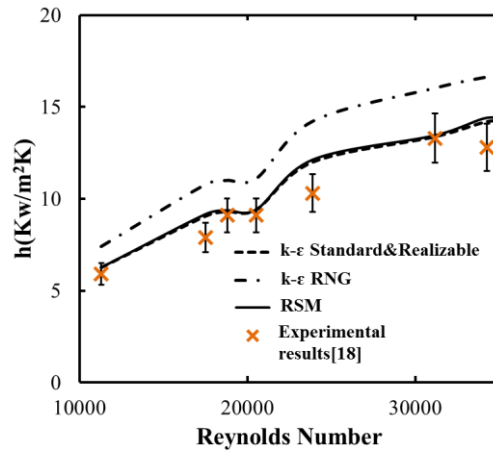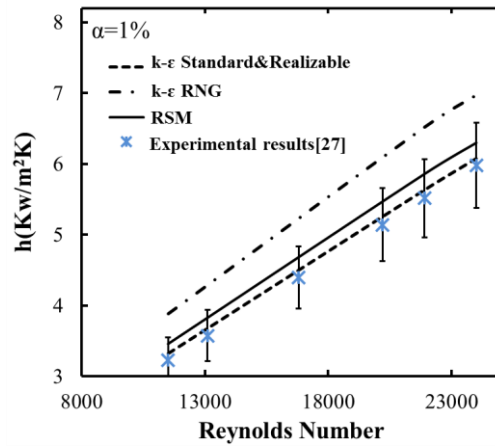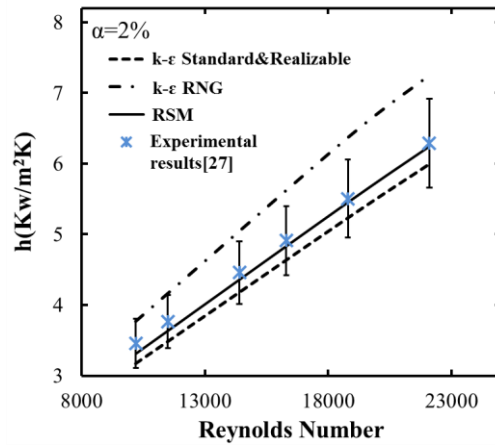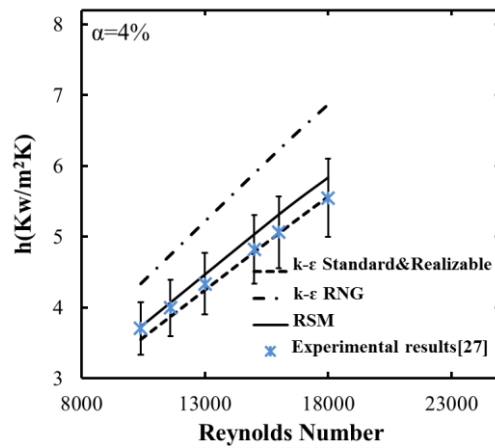
a)

b)

c)

Figure 13: A mixture model prediction of heat transfer coefficient of SiO_2 nanofluid through a heated tube with a different particle loading.

In summary, it can be concluded that the Mixture model can estimate pressure drop and heat transfer characteristics in nanofluid flow in most of the cases if accurate thermophysical properties of the nanofluids are available. Moreover, most of the available nanofluid properties are measured in static situations, while the effects of convective nanofluid have to be considered to determine their thermophysical properties [50].

On the other hand, DPM simulation results show that there is a reasonable trend for all the predictions that come from some weaknesses in the model, especially in the directional distribution of fluctuating terms of velocity. It is worth mentioning that the most important advantage of DPM is the simulation of nanofluid without any extra details from experiments. With the aim of better understanding the capabilities of DPM, the major changes of flow calculated by DPM are discussed in the following section.

3.1 Discussion of DPM predictions

In this section, the other aspects of the DPM simulations are explained. In the first step, it is imperative to understand that the main feature of nanoparticles is the number of particles in each parcel. This implies that, even though the slip velocity and consequent forces between the fluid and the particles are very small, they could nonetheless affect flow field due to the large number of particles in each cell, which is in the order of 10^{10} in this study. All the particles in each computational cell are divided into a number of groups, called parcels, and one particle in each parcel represents all the particles in that parcel. The number of particles in each parcel is available from the following:

$$N_{particle} = \dot{m}_p \frac{\Delta t}{m_p} \tag{37}$$

The order of particle mass in this correlation is $m_p \sim O(10^{-23})$.

It has been revealed that all the forces, including gravity, virtual mass, pressure gradient, thermophoretic, Brownian and lift forces, have no impact on mean flow field or the instantaneous components of the flow. This was found by comparing the hydrodynamic and thermal characteristics of the flow in the presence and absence of those forces in 2D and 3D. Therefore, the only influencing force is the drag force over

the particles, which stemmed from the inertia of the particles. The effects of particles' drag force in the flow are provided in tables 2 and 3. ΔP and Δh are the differences between the pressure drops and heat transfer coefficients in the presence and absence of drag force respectively. P and h are pressure drop and heat transfer coefficient in the presence of drag force. Simulation results explain that the percentage of changes is more sensitive to the increase in particle loading than the Reynolds number value. Therefore, it is expected that the lower limit of the percentage occurs in a lower particle loading. Consequently, the upper limit occurs in higher particle loadings. Because of the anisotropy assumption, the effects of drag force are more visible by RSM predictions, while the k-ω model presented the minimum changes for pressure drop in TiO_2 nanofluid. Due to the lower Reynolds number, the turbulence intensity, which is defined as $I = \dfrac{u'}{u}$, will be reduced. As a result, the Reynolds stress values, in other words, the influences of fluctuating velocity, reduce in comparison to the mean flow velocity. Since TiO_2 nanofluid takes place at the lowest nanoparticle loading and Reynolds number in comparison to the other nanofluids, the drag force shows small effects on pressure drops. Furthermore, the main influences of particles' drag force are excluded from pressure losses and, in fact, the presence of nanoparticles shows no significant impact on heat transfer coefficient in most of the simulations.

It is important to notice that the instantaneous component of velocity plays an outstanding role in nanofluid simulations. Actually, it has been observed that all the changes in pressure and heat transfer in tables 2 and 3 exist if only the effects of fluctuating velocity over the particles are considered by the DRW model. Figure 14 describes the changes in turbulent kinetic energy at the outlet for Al_2O_3 nanofluid on Re = 9 000 in the presence (3.6%) and absence of nanoparticle loading. The higher values and changes for turbulent kinetic energy are expected for RSM compared with the k-ε model because of the anisotropy assumption.

A comparison between particles and flow in axial velocity at the outlet (in Figure 15) indicates that there is a small slip velocity, which mainly happens in the fully turbulent region. The total impacts may not be negligible in the momentum equation because of the large number of nanoparticles in each cell (in the order of 10^{10}). Moreover, the increase in mean flow velocity with the presence of particles by RSM clearly shows that

RSM can capture some of the effects of nanoparticles on mean flow velocity as opposed to the k-ε model.

Table 2: Impact of the presence of nanoparticles' drag force in flow on pressure drop

	$(\frac{\Delta P}{P})_{Al_2O_3}$	$(\frac{\Delta P}{P})_{ZrO_2}$	$(\frac{\Delta P}{P})_{SiO_2}$	$(\frac{\Delta P}{P})_{TiO_2}$
All *k-ε* models	2%–5%	1%–3.5%	1.5%–4%	0.1%–1.3%
RSM	7%–24%	3%–12%	2.5%–12%	1.4%–6%
k-ω	-	-	-	0.1%–0.5%

Table 3: Impact of the presence of nanoparticles' drag force in flow on heat transfer coefficient

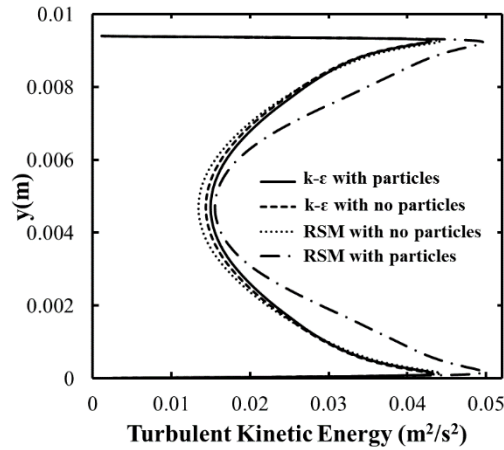|	$(\frac{\Delta h}{h})_{Al_2O_3}$	$(\frac{\Delta h}{h})_{ZrO_2}$	$(\frac{\Delta h}{h})_{SiO_2}$
All *k-ε* models	2%–5%	1%–1.2%	1%–5%
RSM	6%–8%	1%–3%	1%–6%

Figure 14: The effects of nanoparticles on turbulent kinetic energy at flow outlet for Al_2O_3 nanofluid on Re = 9000 with 3.6% volume fraction by RSM and k-ε Standard model.

a)   b)
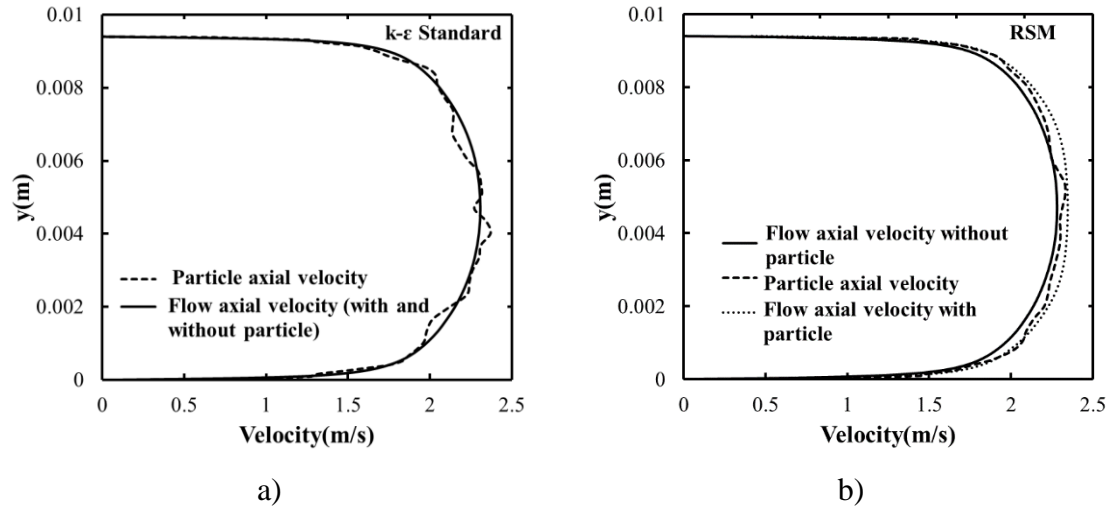
Figure 15: The profile of flow and particle axial velocity at the outlet for Al_2O_3 nanofluid on Re= 9000 with 3.6 % volume fraction predicted by a) k-ε standard model and b) RSM.

4. Conclusions

The abilities and points of weakness of two multiphase flow models were investigated in this research. The simulation results were compared with experimental data available in literature. The k-ε Realisable and Standard models provided the same results in all the simulations. The Mixture model predictions were reasonable for pressure drop in most of the cases in both diabatic and adiabatic tubes, although the results are not satisfactory in some simulations. With the exception of the k-ε RNG model, the heat transfer coefficient predictions of the other turbulence models by the Mixture model showed good agreement with experimental data.

With the DPM approach, the RSM overestimates pressure drop in comparison with k-ε models with higher Reynolds numbers, but both DPM and the RSM model agree with the experimental data with lower Reynolds numbers. Furthermore, there are no changes in the pressure results of the two-equation turbulence model for a TiO_2 nanofluid with a low Reynolds number and an increased nanoparticle loading. Only RSM can predict the rise in pressure drop in a low nanoparticle loading. On the other hand, a similar pattern was revealed for the estimation of heat transfer coefficient. The k-ε RNG model provides poor prediction of the heat transfer coefficient in all simulations. The assumption of anisotropy of fluctuating velocity plays a key role in nanofluid

simulations, as the amount of turbulent kinetic energy and slip velocity between nanoparticles and the main flow by RSM is more in comparison with the k-ε Realisable model.

In summary, it is still challenging to choose the appropriate nanofluids' thermophysical properties for each case, which highly depends on the nanoparticles and base fluids. The mixture model was not able to capture the slip velocity and temperature gap between solid and liquid phases either. Characterising the nature of the thermal and hydrodynamic behaviour of nanofluids is important. Depending on the type and diameter of nanoparticles, DPM provided reliable results for both heat transfer and pressure drop in many cases regarding the uncertainty (such as less than 1.8% for Al_2O_3 and 0.5% for ZrO_2 nanofluids). Furthermore, DPM has shown good abilities to capture slip velocity between phases. Hence, it is highly recommended for these cases. On the other hand, it has to be noted that the nature of nanofluid flow becomes more complicated in higher volume fractions and Reynolds numbers due to the existence of other phenomena like clustering and rapid growth in turbulent perturbations. Therefore, a new study is required for this area as a separate field of nanofluid flow in future works.

Acknowledgements

Nomenclature

A	particle surface area	P	pressure
C_D	drag coefficient	q_m	Conduction diffusion flux
c_p	particle specific heat	q_T	Turbulence diffusion flux
d_p	particle diameter	Q_s	energy source term
D	tube diameter	Re_p	Particle Reynolds number
D_T	Thermophoretic coefficient	St	Stokes number
f	friction factor	Δt	Lagrangian time step
F_B	Brownian force	T	temperature
F_L	Lift force	Δt	Particle time step
F_p	Pressure gradient force		
F_s	momentum source term	*Greek symbols*	
F_T	Thermophoretic force	φ	volume fraction
F_{vm}	Virtual mass force	λ	mean free path
H	enthalpy	μ	viscosity
h	heat transfer coefficient	ρ	density
κ	thermal conductivity	$\vec{\varsigma}$	Gaussian random noise function
K_B	Boltzmann constant	τ	particle relaxation time
Kn	Knudsen number	τ_m	mixture shear stress tensor
k	kinetic energy		
L	Characteristic length	*Subscripts*	
m_p	particle mass	c	continuous or liquid phase
$\dot{m}$	mass flow rate	*in-cell*	inlet of a cell
$N_{particle}$	number of particles	k	phase k
U	characteristic velocity	m	mixture
u'	fluctuating velocity	*out-cell*	outlet of a cell
u_{km}, u_{pm}	drift velocity	p	particle
u_{slip}	relative or slip velocity		
Pr	Prandtl number		

References

1. Lazarus, G.B., Raja, D., Mohan, L., Wongwises, S. Enhancement of heat transfer using nanofluids – an overview. *Renewable Sustainable Energy Reviews*, v. 14, p. 629–641, 2010.

2. Hussein, A.M., Sharma, K.V., Bakar, R.A., Kadirgama, K.A. A review of forced convection heat transfer enhancement and hydrodynamic characteristics of a nanofluid. *Renewable and Sustainable Energy Reviews*, v. 29, p. 734–743, 2014.

3. Sundar, L.S., Singh, M.K. Convective heat transfer and friction factor correlations of nanofluid in a tube and with inserts: a review. *Renewable and Sustainable Energy Reviews*, v. 20, p. 23–35, 2013.

4. Xuan, Y., Li, Q. Heat transfer enhancement of nanofluids. *International Journal of Heat and Fluid Flow*, v. 21, p. 58–64, 2002.

5. Suresh, S., Venkitaraj, K.P., Selvakumar, P., Chandrasekar, M. Effect of Al_2O_3-Cu/water hybrid nanofluid in heat transfer. *Experimental Thermal and Fluid Science*, v. 38, p. 54–60, 2012.

6. Fakoor-Pakdaman, M., Akhavan-Behabadi, M.A., Razi, P. An empirical study on the pressure drop characteristics of nanofluid flow inside helically coiled tubes. *International Journal of Thermal Sciences*, v. 65, p. 206–213, 2013.

7. Ben Mansour, R., Galanis, N., Nguyen, C.T. Experimental study of mixed convection with water-Al_2O_3 nanofluid in inclined tube with uniform wall heat flux. *International Journal of Thermal Sciences*, v. 50, p. 403–410, 2011.

8. Buongiorno, J. Convective transport in nanofluids. *Journal of Heat Transfer*, v. 128, p. 240–250, 2006.

9. Wen, D., Ding, Y. Experimental investigation into convective heat transfer of nanofluids at the entrance region under laminar flow conditions. *International Journal of Heat and Mass Transfer*, v. 47, p. 5181–5188, 2004.

10. Heris, Z., Esfahany, M., Etemad, S. Experimental investigation of convective heat transfer of Al_2O_3/water nanofluid in circular tube. *International Journal of Heat and Fluid Flow*, v. 28, n. 2, p. 203–210, 2007.

11. Faulkner, D., Rector, D.R., Davison, J.J., Shekarriz, R. Enhanced heat transfer through the use of nanofluids in forced convection. *Proceedings of American Society of Mechanical Engineering Conference*, p. 219–224, 2004.

12. Dong, S., Zheng, L., Zhang, X., Wu, S., Shen, B. A new model for Brownian force and the application to simulating nanofluid flow. *Microfluidics and Nanofluidics*, v. 16, p. 131–139, 2014.

13. Xuan, Y., Li, Q. Investigation on convective heat transfer and flow features of nanofluids. *Journal of Heat Transfer*, v. 125, p. 151–155, 2003.

14. Suresh, S., Chandrasekar, M., Sekhar, S. Experimental studies on heat transfer and friction factor characteristics of CuO/water nanofluid under turbulent flow in a helically dimpled tube. *Experimental Thermal and Fluid Science*, v. 35, p. 542–549, 2011.

15. Duangthongsuk, W., Wongwises, S. An experimental study on the heat transfer performance and pressure drop of TiO2-water nanofluids flowing under a turbulent flow regime. *International Journal of Heat and Mass Transfer*, v. 53, p. 334–344, 2010.

16. Kakaç, S., Pramuanjaroenkij, A. Review of convective heat transfer enhancement with nanofluids. *International Journal of Heat and Mass Transfer*, v. 52, p. 3187–3196, 2009.

17. Heyhat, M.M., Kowsary, F., Rashidi, A.M., Esfehani, S., Alem, V., Amrollahi, A. Experimental investigation of turbulent flow and convective heat transfer characteristics of alumina water nanofluids in fully developed flow regime. *International Communications in Heat and Mass Transfer*, v. 39, p. 1272–1278, 2012.

18. Williams, W., Buongiorno, J., Hu, L-W. Experimental investigation of turbulent convective heat transfer and pressure loss of alumina/water and zirconia/water nanoparticle colloids (nanofluids) in horizontal tubes. *Journal of Heat Transfer*, v. 130, p. 7, 2008.

19. Ibrahim, W., Makinde, O.D. The effect of double stratification on boundary-layer flow and heat transfer of nanofluid over a vertical plate. *Computers and Fluids*, v. 86, p. 433–441, 2013.

20. Rosca, N.C., Pop, I. Unsteady boundary layer flow of a nanofluid past a moving surface in an external uniform free stream using Buongiorno's model. *Computers and Fluids*, v. 95, p. 49–55, 2014.

21. Zhang, Y., Li, L., Ma, H.B., Yang, M. Effects of Brownian and thermophoretic diffusions of nanoparticles on nonequilibrium heat conduction in a nanofluid layer with periodic heat flux. *Numerical Heat Transfer Part A: Applications*, v. 56, p. 325–341, 2009.

22. Laín, S., Sommerfeld, M. Numerical calculation of pneumatic conveying in horizontal channels and pipes: detailed analysis of conveying behaviour. *International Journal of Multiphase Flow*, v. 39, p. 105–120, 2012.

23. Bianco, V., Manca, O., Nardini, S. Numerical investigation on nanofluids turbulent convection heat transfer inside a circular tube. *International Journal of Thermal Sciences*, v. 50, p. 341–349, 2011.

24. Lotfi, R., Saboohi, Y., Rashidi, A.M. Numerical study of forced convective heat transfer of nanofluids: comparison of different approaches. *International Communications in Heat and Mass Transfer*, v. 37, p. 74–78, 2010.

25. Nwosu, P.N., Meyer, J., Sharifpur, M. Nanofluid viscosity: a simple model selection algorithm and parametric evaluation. *Computers and Fluids*, v. 101, p. 241–249, 2014.

26. Huilier, D. On the necessity of including the turbulence experienced by an inertial particle in Lagrangian random walk models. *Mechanics Research Communications*, v. 31, p. 237–242, 2004.

27. Azmi, W.H., Sharma, K.V., Sarma, P.K., Mamat, R., Anuar, S., Rao, V.D. Experimental determination of turbulent forced convection heat transfer and friction factor with SiO_2 nanofluid. *Experimental Thermal and Fluid Science*, v. 51, p. 103–111, 2013.

28. Teng, T.P., Hung, Y., Jwo, C.S, Chen, C-C., Jeng, L-Y. Pressure drop of TiO_2 nanofluid in circular pipes. *Particuology*, v. 9, p. 486– 491, 2011.

29. Kaushal, D.R., Thinglas, T., Tomita, Y., Kuchii, S., Tsukamoto, H. CFD modeling for pipeline flow of fine particles at high concentration. *International Journal of Multiphase Flow*, v. 43, p. 85–100, 2012.

30. Mahdavi, M., Sharifpur, M., Meyer, J.P. CFD modelling of heat transfer and pressure drops for nanofluids through vertical tubes in laminar flow by Lagrangian and Eulerian approaches. *International Journal of Heat and Mass Transfer*, v. 88, p. 803-813, 2015.

31. Schiller, L., Naumann, A. A drag coefficient correlation. *Zeitschrift Des Vereines Deutscher Ingenieure*, v. 77, p. 318–320, 1935.

32. Marshall, J.S., Li, S. *Adhesive particle flow: a discrete-element approach* (First edition). Cambridge University Press, New York, NY, Chapter 5, 2014.

33. Morsi, S.A., Alexander, A.J. An investigation of particle trajectories in two-phase flow systems. *Journal of Fluid Mechanics*, v. 55, n. 2, p. 193–208, 1972.

34. Haider, A., Levenspiel, O. Drag coefficient and terminal velocity of spherical and nonspherical particles. *Powder Technology*, v. 58, 63–70, 1989.

35. McNab, G.S., Meisen, A. Thermophoresis in liquids. *Colloid Interface Science*, v. 44, n. 2, p. 339–346, 1973.

36. Minkowycz, W.J., Sparrow, E.M., Murthy, J.Y. *Handbook of numerical heat transfer* (Second edition). Hoboken, NJ, Wiley, p. 701, 2006.

37. Bayazit, M. Random walk model for motion of a solid particle in turbulent open-channel flow. *Journal of Hydraulic Research*, v. 10, n. 1, p. 1–13, 1972.

38. Strutt, H.C., Lightstone, M.F. Analysis of tracer particle migration in inhomogeneous turbulence. *International Journal of Heat and Mass Transfer*, v. 49, p. 2557–2566, 2006.

39. Chao, C.Y.H., Wan, M.P. A study of the dispersion of expiratory aerosols in unidirectional downward and ceiling-return type airflows using a multiphase approach. *Indoor Air*, v. 16, p. 296–312, 2006.

40. Shuen, J.S., Chen, L.D., Faeth, G.M. Evaluation of a stochastic model of particle dispersion in a turbulent round jet. *AIChE Journal*, v. 29, p. 167–170, 1983.

41. Williams, W.C. Experimental and theoretical investigation of transport phenomena in nanoparticle colloids (nanofluids). PhD thesis, Massachusetts Institute of Technology, p. 136–137, 2007.

42. Mandar, V.T., Swarnendu, A.R., Jyeshtharaj, B.J. CFD simulation of bubble column – an analysis of interphase forces and turbulence models. *Chemical Engineering Journal*, v. 139, n. 3, p. 589–614, 2008.

43. Boutet, C.L., Larachi, F., Dromard, N., Delsart, O., Schweich, D. CFD simulation of bubble column flows: investigations on turbulence models in RANS approach. *Chemical Engineering Science*, v. 64, n. 21, p. 4399–4413, 2009.

44. Suryana, A., Kim, H.D., Setoguchi, T. Comparative study of turbulence models performance for refueling of compressed hydrogen tanks. *International Journal of Hydrogen Energy*, v. 38, p. 9562–9569, 2013.

45. Rocha, P.A.C., Barbosa, H.H., Carneiro, F.O.M., Silva, M.E., Bueno, A.V. Ke-w SST (shear stress transport) turbulence model calibration: a case study on a small scale horizontal axis wind turbine. *Energy*, v. 65, p. 412–418, 2014.

46. Wang, Q., Squires, K.D. Large eddy simulation of particle deposition in a vertical turbulent channel flow. *International Journal of Multiphase Flow*, v. 22, n. 4, p. 667–683, 1996.

47. Sijercic, M., Belosevic, S., Stevanovic, Z. Simulation of free turbulent particle-laden jet using Reynolds stress gas turbulence model. *Applied Mathematical Modelling*, v. 31, p. 1001–1014, 2007.

48. Schlichting, H., Gersten, K. *Boundary-layer theory.* [s.l.], Springer, Chapter 2, p. 37, 2000.

49. FLUENT15. *User manual.* Fluent Incorporated, 2014.

50. Kolade, B., Goodson, K.E., Eaton, J.K. Convective performance of nanofluids in a laminar thermally developing tube flow. *Journal of Heat Transfer*, v. 131, n. 5, p. 1–8, 2009.